minerals

MDPI

Article

Polytypism of Compounds with the General Formula $Cs\{Al_2[TP_6O_{20}]\}$ (T = B, Al): OD (Order-Disorder) Description, Topological Features, and DFT-Calculations

Sergey M. Aksenov [1,2,*], Alexey N. Kuznetsov [3,4], Andrey A. Antonov [1], Natalia A. Yamnova [5], Sergey V. Krivovichev [6,7] and Stefano Merlino [8]

1 Laboratory of Nature-Inspired Technologies and Environmental Safety of the Arctic, Kola Science Centre, Russian Academy of Sciences, 14 Fersman str., 184209 Apatity, Russia; a.antonov@ksc.ru
2 Geological Institute of Kola Science Centre, Russian Academy of Sciences, 14 Fersman Street, 184209 Apatity, Russia
3 Faculty of Chemistry, Moscow State University, Vorobievy Gory, 119991 Moscow, Russia; alexei@inorg.chem.msu.ru
4 Kurnakov Institute of General and Inorganic Chemistry RAS, Leninskii pr. 31, 119991 Moscow, Russia
5 Faculty of Geology, Moscow State University, Vorobievy Gory, 119991 Moscow, Russia; natalia-yamnova@yandex.ru
6 Nanomaterials Research Centre of Kola Science Centre, Russian Academy of Sciences, 14 Fersman Street, 184209 Apatity, Russia; skrivovi@mail.ru
7 Department of Crystallography, Institute of Earth Sciences, Saint–Petersburg State University, University Emb. 7/9, 199034 St. Petersburg, Russia
8 Accademia Nazionale dei Lincei, 00165 Rome, Italy; stefano.merlino38@gmail.com
* Correspondence: aks.crys@gmail.com

check for updates

Citation: Aksenov, S.M.; Kuznetsov, A.N.; Antonov, A.A.; Yamnova, N.A.; Krivovichev, S.V.; Merlino, S. Polytypism of Compounds with the General Formula $Cs\{Al_2[TP_6O_{20}]\}$ (T = B, Al): OD (Order-Disorder) Description, Topological Features, and DFT-Calculations. *Minerals* **2021**, *11*, 708. https://doi.org/10.3390/min11070708

Academic Editor: Giovanni Ferraris

Received: 12 June 2021
Accepted: 28 June 2021
Published: 30 June 2021

Abstract: The crystal structures of compounds with the general formula $Cs\{^{[6]}Al_2[^{[4]}TP_6O_{20}]\}$ (where T = Al, B) display order-disorder (OD) character and can be described using the same OD groupoid family. Their structures are built up by two kinds of nonpolar layers, with the layer symmetries $Pc(n)2$ (L_{2n+1}-type) and $Pc(a)m$ (L_{2n}-type) (category IV). Layers of both types (L_{2n} and L_{2n+1}) alternate along the **b** direction and have common translation vectors **a** and **c** (a ~ 10.0 Å, c ~ 12.0 Å). All ordered polytypes as well as disordered structures can be obtained using the following partial symmetry operators that may be active in the L_{2n} type layer: the 2_1 screw axis parallel to **c** [$--2_1$] or inversion centers and the 2_1 screw axis parallel to **a** [2_1--]. Different sequences of operators active in the L_{2n} type layer ([$--2_1$] screw axes or inversion centers and [2_1--] screw axes) define the formation of multilayered structures with the increased b parameter, which are considered as non-MDO polytypes. The microporous heteropolyhedral MT-frameworks are suitable for the migration of small cations such as Li^+, Na^+ Ag^+. Compounds with the general formula $Rb\{^{[6]}M^{3+}[^{[4]}T^{3+}P_6O_{20}]\}$ (M = Al, Ga; T = Al, Ga) are based on heteropolyhedral MT-frameworks with the same stoichiometry as in $Cs\{^{[6]}Al_2[^{[4]}TP_6O_{20}]\}$ (where T = Al, B). It was found that all the frameworks have common natural tilings, which indicate the close relationships of the two families of compounds. The conclusions are supported by the DFT calculation data.

Keywords: OD structures; polytypism; polymorphism; heteropolyhedral framework; modularity; topology; borophosphates; aluminophosphates; DFT

1. Introduction

Borophosphates (as well as borophosphate ceramics and glasses) attract interest because of their wide technological applications as materials with optical [1–5], electrochemical [6–9], magnetic [10–12], and catalytic [13–15] properties. Moreover, crystalline borophosphates and metal borophosphates with microporous structures are considered as zeolite-like materials [16–20]. Borophosphates are characterized by a wide diversity of tetrahedral and mixed triangular-tetrahedral anionic motifs [21–24], owing to the different

possible coordination environments of boron. At present, more than 300 representatives of this class are known, which are characterized by anionic motifs with different dimensionalities (from isolated groups to 3D frameworks).

Compounds with the general formula $Cs\{^{[6]}Al_2[^{[4]}TP_6O_{20}]\}$ (where T = B [25], Al [26]) are based on microporous heteropolyhedral frameworks formed by tetrahedral borophosphate or aluminophosphate $[TP_6O_{20}]$-layers linked by isolated AlO_6 octahedra. The large framework cavities are filled by Cs^+ cations. As was previously shown, both $Cs\{Al_2[BP_6O_{20}]\}$ and $Cs\{Al_2[AlP_6O_{20}]\}$ are of modular character [27] and can be considered as polytypes belonging to the same OD family [20,25]. However, the corresponding groupoid family has not been reported so far.

In this paper we provide a complete OD-theoretical analysis of the compounds with the general formula $Cs\{^{[6]}Al_2[TP_6O_{20}]\}$ (where T = B [25], Al [26]) and derive symmetry and atom coordinates for the hypothetical MDO2 polytype. The energies of the observed and hypothetical structures of the family are calculated using the density functional theory (DFT). Possible ion-migration paths inside the microporous frameworks of the family are estimated for different alkaline ions using the topological analysis.

2. Methods

The symmetrical relations between the compounds have been analyzed using the OD theoretical approach [27–30] for the OD families containing more than one ($M > 1$) kind of layers [31]. The OD layers have been chosen in accordance with the equivalent region (ER) requirements [32]. As a reference structure for the further analysis, the MDO1 polytype observed in $Cs\{Al_2[AlP_6O_{20}]\}$ [26] was used. This compound was reported in the non-standard setting of the space group *C*2*cb* [a = 10.0048(7) Å, b = 13.3008(10) Å, c = 12.1698(7) Å], which was transformed into the standard setting *Aea*2 using the [00–1/010/100] matrix (the resulting unit cell parameters are: a = 12.1698(7) Å b = 13.3008(10) Å, c = 10.0048(7) Å). The unit-cell parameters and space groups of the crystal structures of $Cs\{Al_2[BP_6O_{20}]\}$ polytypes have been transformed accordingly in order to preserve the orientation and stacking direction of the OD-layers.

Topological analysis of the frameworks was performed by means of natural tilings (the smallest polyhedral cationic clusters that form a framework) of the 3D cation nets [33]. The complexity parameters of the frameworks in different polytypes were calculated as Shannon information amounts per atom (I_G) and per reduced unit cell ($I_{G,total}$) [34,35]. To analyze the migration paths of alkaline cations in the structures, the Voronoi method [36], which has proven itself in the study of cationic conductors of various types [37,38], was used. Topological and complexity parameters for the whole structures as well as ion migration paths have been calculated using the ToposPro software [39].

DFT calculations on the existing MDO-, non-MDO-4*O*, as well as hypothetical MDO2 type polytypes (T = Al, B) were performed using the PBE exchange-correlation functional [40] of the GGA-type utilizing the projector augmented wave method (PAW) as implemented in the Vienna ab initio simulation package (VASP) [41,42]. The energy cut-off was set at 500 eV with a 10 × 8 × 8 (MDO1, MDO2), and 6 × 4 × 4 (non-MDO-4*O*) Monkhorst−Pack [43] k-point mesh used for Brillouin zone sampling. The convergence towards the k-point mesh was checked. Full optimization of the unit cell parameters and atomic coordinates was performed for all the structures except the MDO1 polytype of $Cs\{Al_2[BP_6O_{20}]\}$, for which the original cell parameters were retained and atomic coordinates optimized (as the compound was found to have the lowest energy, cell parameter optimization was deemed unnecessary). For the optimization, the structures were converted to the space group *P*1.

3. Results

3.1. OD (Order-Disorder) Relationships

The crystal structures of $Cs\{^{[6]}Al_2[^{[4]}TP_6O_{20}]\}$ (where T = B [25], Al [26]) belong to the same OD family of category IV [31] with two types of nonpolar OD layers and can be described by an OD groupoid [27]. The layers are as following:

1. Nonpolar L_{2n+1} type with the layer symmetry *pcn*2 [or *Pc*(*n*)2 in terms of the OD notation, where braces indicate the direction of missing periodicity [44]] was reported previously [20] and is represented by the tetrahedral $[^{[4]}TP_6O_{20}]$-layer (Figure 1);
2. Nonpolar L_{2n} type consists of aluminum and oxygen atoms on the borders of a thin slab with the layer symmetry *pcam* [*Pc*(*a*)*m* or $P2_1/c$ $(2/a)$ $2_1/m$].

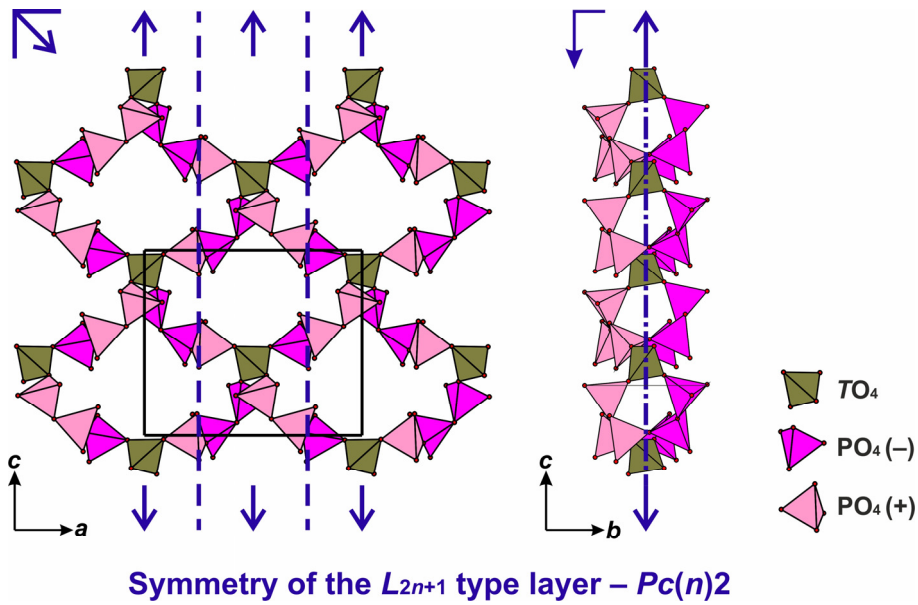

Figure 1. The general view of the tetrahedral L_{2n+1} type layer in the crystal structures of $Cs\{^{[6]}Al_2[^{[4]}TP_6O_{20}]\}$ polytypes. The fundamental building block (FBB) of the layer is represented by open-branched heptamer with the following descriptor [21,45]: 7□:[3□]2□|2□|□|□. Modified after [20].

Layers of both types (L_{2n} and L_{2n+1}) alternate along the **b** direction and have common translation vectors **a** and **c** (a ~ 10.0 Å, c ~ 12.0 Å), with b_0, the distance between the two nearest equivalent layers, corresponding to one half of the b parameter of the compound studied by Lesage et al. [26]. Because the symmetry of the L_{2n} type layers is higher than that of the L_{2n+1} type layers, polytypic relations are possible. All ordered polytypes as well as disordered structures can be obtained using the following symmetry operators that may be active in the L_{2n} type layer: the 2_1 screw axis parallel to **c** [– – 2_1] or inversion centers and the 2_1 screw axis parallel to **a** [2_1 – –] (Figure 2) [20]. The symmetry relation common to all polytypes of this family are described by the OD groupoid family symbol:

$$\begin{matrix} Pc(n)2 & & P\,2_1/c\,(2/a)\,2_1/m \\ & [r,\,0] & \end{matrix}, \quad (1)$$

where r = 0; the first line contains the layer-group symbols of the two constituting layers, while the second line indicates positional relations between the adjacent layers [46].

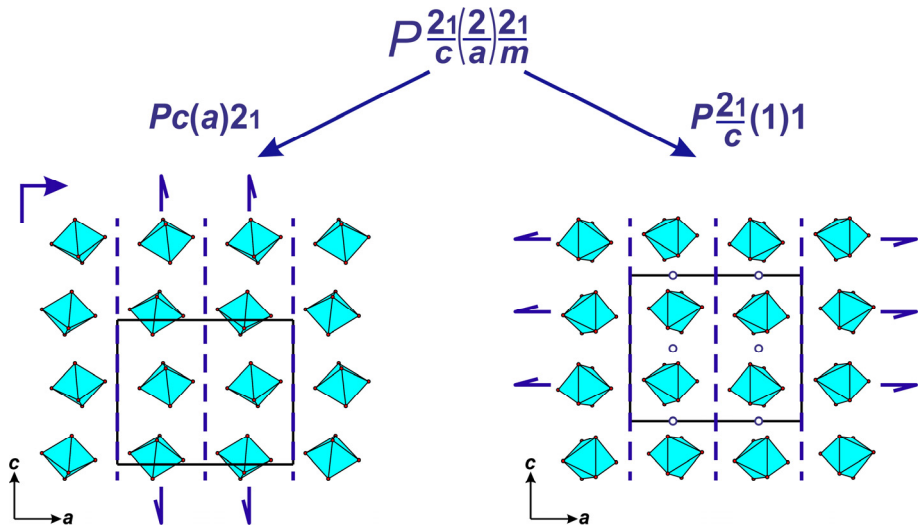

Figure 2. Different symmetry operators that may be active in the L_{2n} type layer: the 2_1 screw axis parallel to **c** [– – 2_1] (**left**) and inversion centers and the 2_1 screw axis parallel to **a** [2_1 – –] (**right**).

In accordance with the *NFZ* relation [27,28], there is only one kind of the (L_{2n}, L_{2n+1}, L_{2n+2}) triples and two kinds of the (L_{2n-1}, L_{2n}, L_{2n+1}) triples. Consequently, the smallest possible number of different triples in a structure is two and only two MDO polytypes are possible:

$$\begin{array}{ccccccc} \text{OD} - \text{layer} & \text{Layer group} & \text{Subgroup of } \lambda\text{-}\tau\text{-operations} & N & F & Z & \\ \mathrm{A}^1 = L_{2n} & P\,2_1/c\,2/a\,2_1/m & P\,c\,2\,m & 4\searrow & & \nearrow 1 & \\ & \text{Symmetry of a layer pair} \rightarrow & P\,c\,1\,1 & & 2 & & , \\ \mathrm{A}^2 = L_{2n+1} & P\,c\,n\,2 & P\,c\,1\,1 & 2\nearrow & & \searrow 2 & \end{array} \quad (2)$$

The first MDO structure (MDO1 polytype) (Figure 3, left) can be obtained when the [– – 2_1] operator is active in L_{2n} type layer. Through the action of this operator the asymmetric unit at x, y, z (I) is converted into the asymmetric unit at $-x$, $\frac{1}{2}-y$, $\frac{1}{2}+z$ (II); the latter unit is converted by the [– – 2] operator in the L_{2n+1} layer into the asymmetric unit at x, $\frac{1}{2}+y$, $\frac{1}{2}+z$ (III). I and III are related by the translation vector $\mathbf{t} = \mathbf{b}_0 + \mathbf{c}/2$, which is the generating operation, giving rise by the continuation to an *A*-centered structure with the basis vectors **a**, $\mathbf{b} = 2\mathbf{b}_0$, **c** and the space group *Aea*2. The MDO1 polytype corresponds to the structure of $Cs\{Al_2[AlP_6O_{20}]\}$ with the following unit cell parameters: a = 12.1698(7) Å b = 13.3008(10) Å, c = 10.0048(7) Å [26].

The second MDO structure (MDO2 polytype) (Figure 3, right) can be obtained when the inversion centers and [2_1 – –] operators are both active in the L_{2n} type layer. Through the action of the operator [2_1 – –] the asymmetric unit at x, y, z (I) is converted into the asymmetric unit $\frac{1}{2}+x$, $-y$, $\frac{1}{2}-z$ (II); the latter unit is converted by the [– n –] operator in the L_{2n+1} layer into the asymmetric unit x, $\frac{1}{2}+y$, $-z$ (III); (I) and (III) are related by a b glide normal to **c**, with translational component b_0, which is the generating operation: its continuation also generates an orthorhombic structure with the basis vectors **a**, $\mathbf{b} = 2\mathbf{b}_0$, **c** (the same for the MDO1 polytype) and the space group *Pcnb* (or *Pbcn* in the standard setting). The MDO2 polytype has not yet been observed for the compound with the general formula $Cs\{^{[6]}Al_2[^{[4]}TP_6O_{20}]\}$. The calculated atomic coordinates for the MDO2 polytype are given in Table S1 (Supplement Materials).

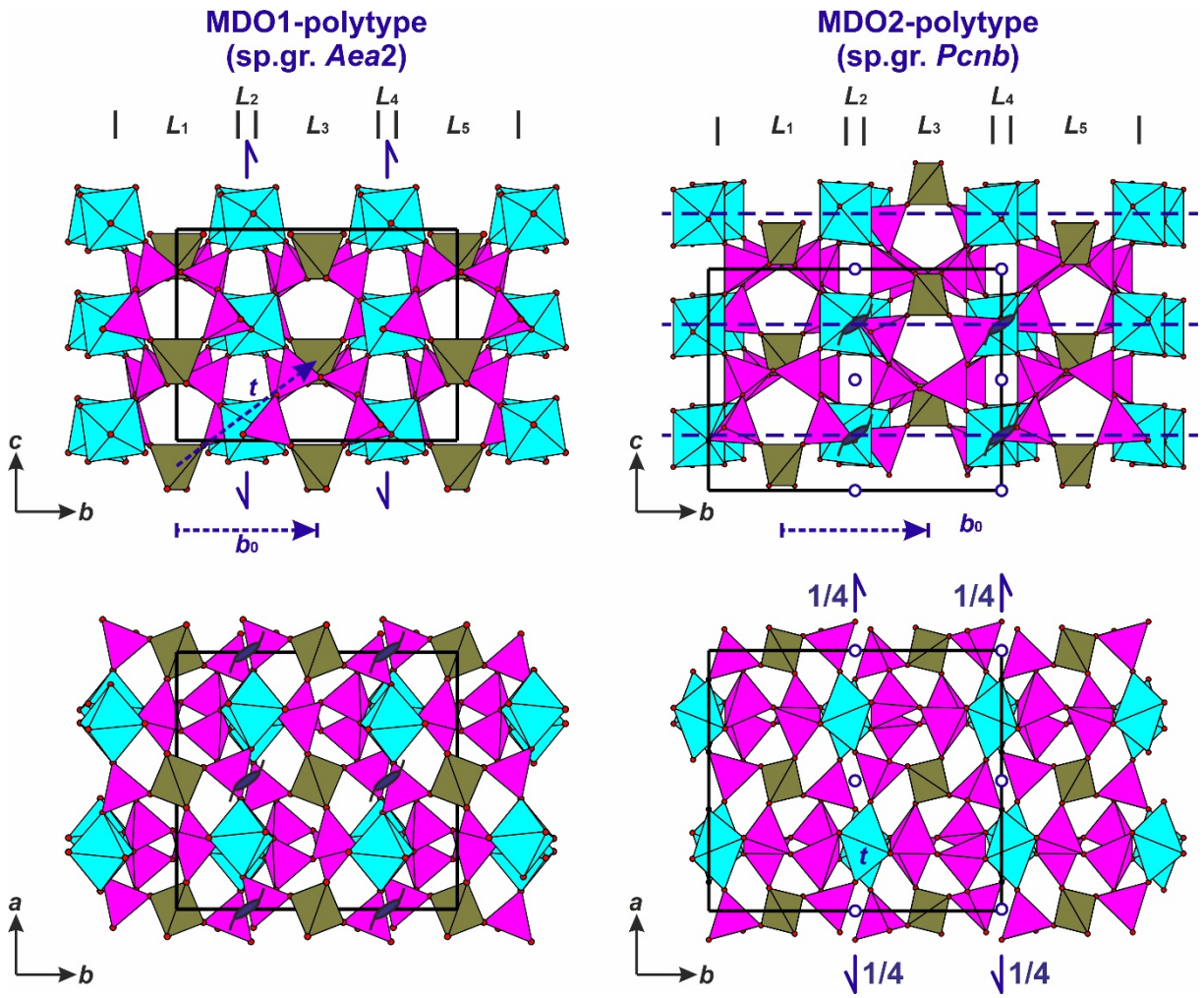

Figure 3. The general views of the MDO1 (with the space group *Aea*2) and MDO2 (with the space group *Pcnb*) polytypes. The operations active in the L_{2n} type layers as well as the generating operations are shown. Legend: AlO_6-octahedra are colored in cyan; PO_4-tetrahedra are colored in purple; TO_4-tetrahedra are colored in dark yellow. Extra-frameworks Cs atoms are omitted.

Different sequences of operators active in the L_{2n} type layer ([– – 2_1] screw axes or inversion centers and [2_1 – –] screw axes) define the formation of structures with the increased *b* parameter, which are considered as non-MDO polytypes (because of the presence of more than one kind of (L_{2n-1}, L_{2n}, L_{2n+1}) triples) [27]. The compound $Cs\{Al_2[BP_6O_{20}]\}$ [25] contains four L_{2n} and L_{2n+1} types layers, where each L_{4n} type layer has active [2_1 – –] screw axes, while in the L_{4n+2} type the inversion centers and [– – 2_1] screw axes are active (Figure 4). The AlO_6 octahedra in the L_{2n+2} and L_{2n+4} type layers are tilted slightly differently, which can be explained by the "desymmetrization" effect of OD structures [27,47,48], when the ideal symmetry suffers slight (in some cases severe) distortions and the symmetry of OD layers in the polytype is lower than the idealized one. The orthorhombic structure of $Cs\{Al_2[BP_6O_{20}]\}$–4*O* is characterized by the basis vectors **a**, **b** = 4$\mathbf{b}_0$, **c** (where *a* = 11.815(2) Å, *b* = 26.630(4) Å, *c* = 10.042(2) Å [25]) and the space group *Pcab* (nonstandard setting of the space group *Pbca*).

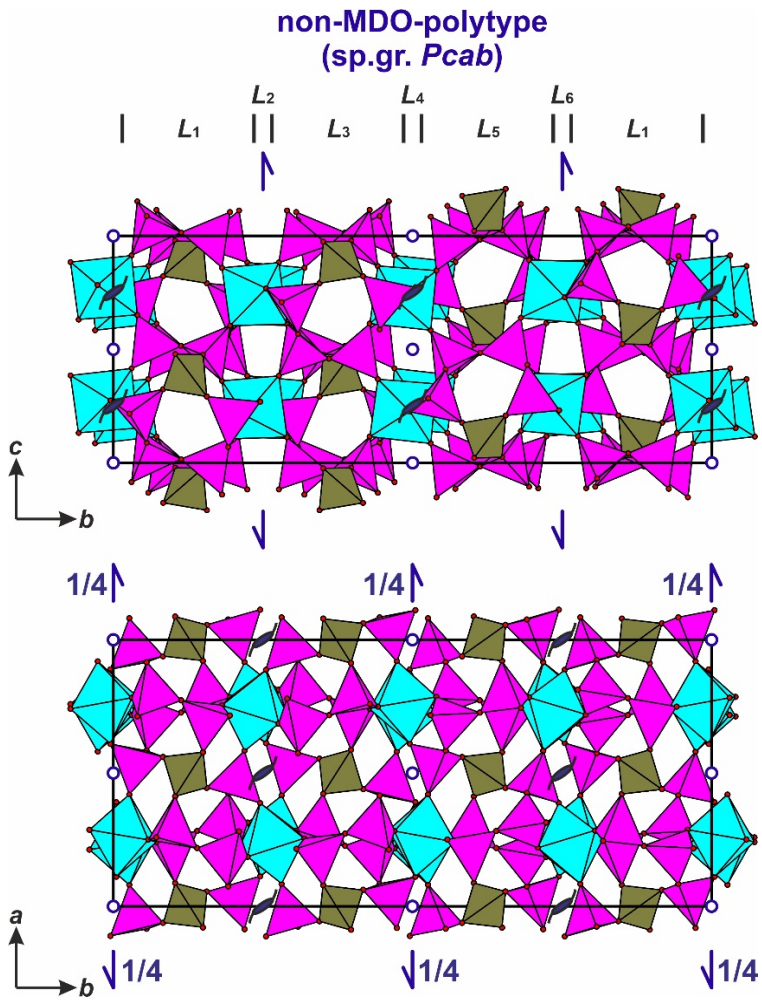

Figure 4. The general views of the non-MDO 4*O* polytype. The operations active in the L_{2n} type layers are shown. Modified after [20].

3.2. Topological Features

Compounds with the general formula $Cs\{^{[6]}Al_2[^{[4]}TP_6O_{20}]\}$ (where T = B [25], Al [26]) are characterized by the heteropolyhedral *MT*-frameworks [20,49–51] of MO_6-octahedra and TO_4-tetrahedra related to classic zeolites and zeolite-type materials where all oxygen ligands are bridged between two cations only [52]. In accordance with the theory of mixed anionic radicals [53–55], the general crystal chemical formula of the framework (taking into account the degree of sharing of oxygen ligands) can be written as [20]:

$$\left\{M_m\left[(T_1)_{n_1}(T_2)_{n_2}O_{3m+2(n_1+n_2)}\right]\right\}^{m(V_M-6)+n_1(V_{T_1}-4)+n_2(V_{T_2}-4)}, \quad (3)$$

where where m and n_i, V_M and V_{T_i} are the valences of the M and T_i cations, respectively. If $M = M^{3+}$, $T_1 = T^{3+}$, $T_2 = P^{5+}$, m = z, $n_1 = y$, $n_2 = z$, the Formula (3) can be rewritten as:

$$\left\{M_x\left[T_yP_zO_{3x+2(y+z)}\right]\right\}^{-3x-y+z}. \quad (4)$$

Taking into account the observed ratio between the x, y, and z coefficients, the stoichiometry of the heteropolyhedral *MT*-framework is:

$$\{M_2[TP_6O_{20}]\}^{1-}. \quad (5)$$

Topological features of the MDO1 and non-MDO 4*O* polytypes have been described previously [20]. The cationic 3D net corresponding to the heteropolyhedral *MT*-framework of MDO2 polytype consists of four natural tiles (Figure 5): $[4.6^2]_2[3.5.6^2]_2[4^4.5^2.7^2][3^2.4^2.6^6.7^2]$. The (6*T*1*M*)-$[4.6^2]$ and (6*T*2*M*)-$[3.5.6^2]$ tiles are topologically equal to those observed in the MDO1 and non-MDO 4*O* polytypes; the (10*T*4*M*)-$[4^4.5^2.7^2]$ tile is equal to that in the non-MDO 4*O* polytype. The (16*T*6*M*)-$[3^2.4^2.6^6.7^2]$ tile is unique and is present in the MDO2 polytype only (Table 1).

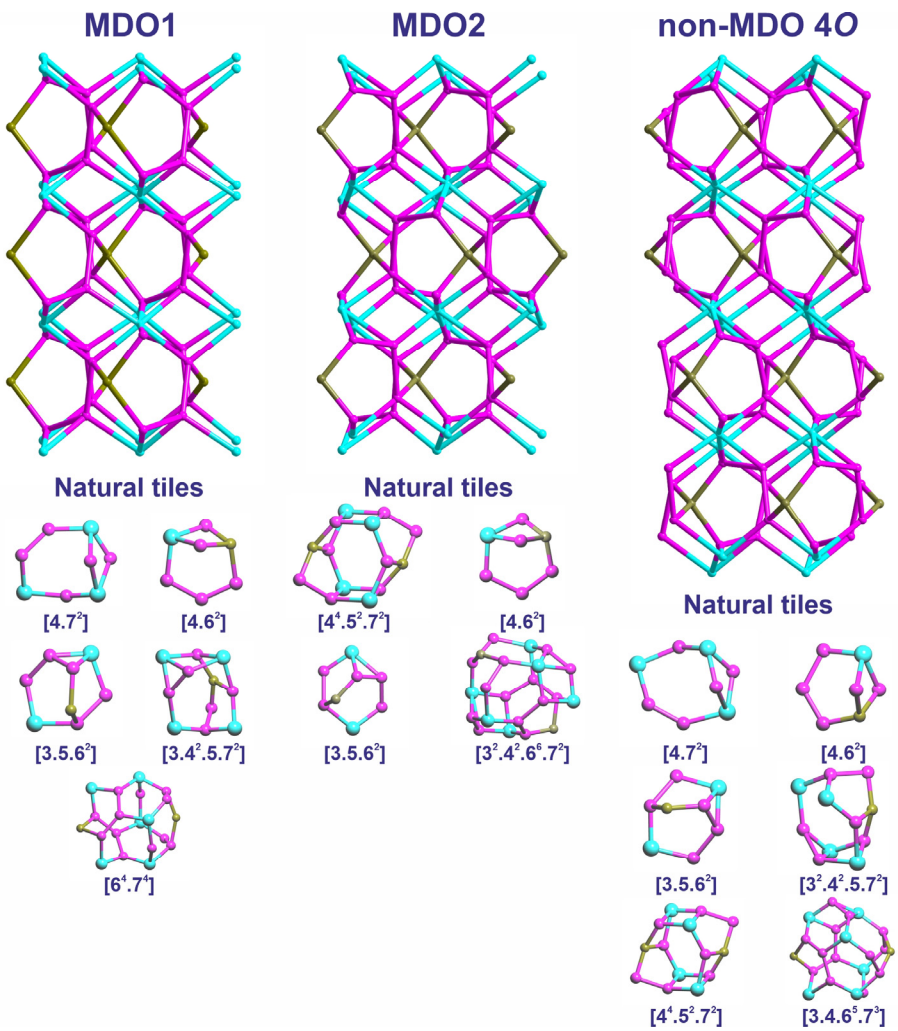

Figure 5. Topological features of the 3D cationic nets of the heteropolyhedral *MT*-frameworks in the structures of MDO1, MDO2 and non-MDO 4O polytypes of compounds with the general formula $Cs\{^{[6]}Al_2[^{[4]}TP_6O_{20}]\}$ (where *T* = B, Al).

Table 1. The natural tiles in the *MT*-frameworks of the polytypes of compounds with the general formula $Cs\{^{[6]}Al_2[^{[4]}TP_6O_{20}]\}$ (where *T* = B, Al).

Polytype	Natural Tiles					
MDO1	$[4.6^2]_2$	$[3.5.6^2]_2$	$[6^4.7^4]$	$[3.4^2.5.7^2]_2$	$[4.7^2]_2$	
MDO2	$[4.6^2]_2$	$[3.5.6^2]_2$	$[4^4.5^2.7^2]$	$[3^2.4^2.6^6.7^2]$		
non-MDO 4*O*	$[4.6^2]_4$	$[3.5.6^2]_4$	$[4^4.5^2.7^2]$	$[3.4^2.5.7^2]_2$	$[4.7^2]_2$	$[3.4.6^5.7^3]_2$

Note. The point symbol of the 3D net has the form $A^a.\ B^b\ \ldots$ indicating that there are *a* angles with shortest cycles that are *A*-cycles, *b* angles with shortest cycles that are *B*-cycles, etc., with $A < B, < \cdots$ and $a + b + \cdots = n(n-1)/2$ [33]. The topologically equivalent tiles are colored in the same color.

The complexity parameters of the heteropolyhedral *MT*-framework of MDO2 polytype are: v = 116 atoms; I_G = 3.892 bits/atom; $I_{G,total}$ = 451.526 bits/unit cell. The complexity parameters increase in the row MDO1 → MDO2 → non-MDO 4*O*.

3.3. Ion Migration Path

Migration maps of Na^+ cation were constructed for the MDO1, MDO2, and non-MDO 4*O* polytypes (Table 2). Despite the presence of large pores filled by large Cs^+ ions, the size of the effective windows between them is not enough for the migration of large alkaline cations. However, all the types of the microporous heteropolyhedral *MT*-framework are suitable for the migration of smaller ions such as Li^+, Na^+ Ag^+. The types of migration maps depend on the topological type of the MT-framework (Figure 6), in particular, for Na^+ ions, the maps are represented by 2D layers parallel to (100) for the MDO1 and non-MDO 4*O* polytypes, while for the MDO2 polytype it is represented by the system of parallel 1D channels directed along [010] (Figure 6). In the case of Li^+ ions, the migration 3D maps are similar for all the types of the frameworks.

Table 2. The natural tiles in the *MT*-frameworks of the polytypes of compounds with the general formula $Cs\{^{[6]}Al_2[^{[4]}TP_6O_{20}]\}$ (where *T* = B, Al).

Polytype	Natural Tiles					
	Li^+	Na^+	Ag^+	K^+	Rb^+	Cs^+
MDO1	3D	2D	2D	–	–	–
MDO2	3D	1D	1D	–	–	–
non-MDO 4*O*	3D	2D	2D	–	–	–

Note: The following significance criteria for elementary channels (R_{chan}) and voids (R_{sd}) have been used for the construction of migration maps: Li^+ (R_{chan} = 2.02 Å; R_{sd} = 1.38 Å); Na^+ (R_{chan} = 2.16 Å; R_{sd} = 1.54 Å); Ag^+ (R_{chan} = 2.20 Å; R_{sd} = 1.58 Å), K^+ (R_{chan} = 2.30 Å; R_{sd} = 1.70 Å); Rb^+ (R_{chan} = 2.38 Å; R_{sd} = 1.78 Å); Cs^+ (R_{chan} = 2.47 Å; R_{sd} = 1.88 Å).

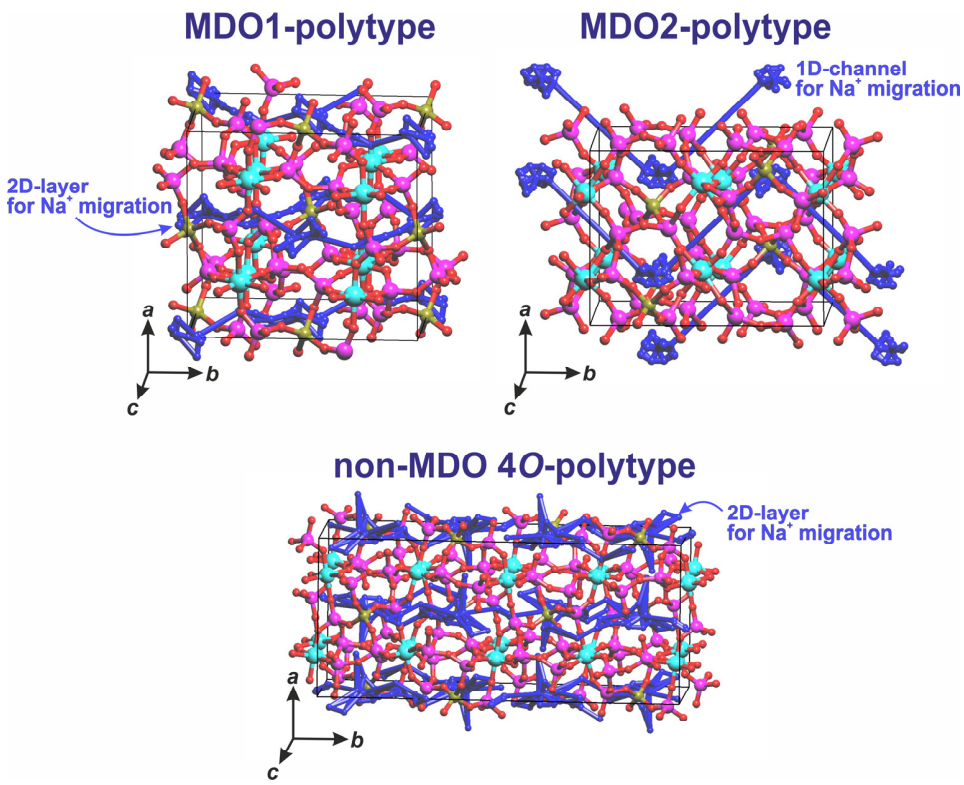

Figure 6. Possible ion migration path of Na^+ cations in the crystal structures of $Cs\{^{[6]}Al_2[^{[4]}TP_6O_{20}]\}$ polytypes.

3.4. DFT Calculations

In order to gain more insight into the stability of various polytypes, energy-wise, we have performed DFT calculations on the existing as well as hypothetical compounds with the general formula $Cs\{Al_2[TP_6O_{20}]\}$ (T = Al, B) with the structures belonging to MDO1, MDO2, and non-MDO 4O type polytypes, for T = Al; B. The comparative data and optimized unit cell parameters are given in Table 3 (for MDO1, T = Al, original unit cell metrics were retained).

Table 3. Comparative data for the frameworks of different polytypes.

Parameter	MDO1 Polytype		MDO2 Polytype		Non-MDO 4*O* Polytype	
	***T* = B**	***T* = Al**	***T* = B**	***T* = Al**	***T* = B**	***T* = Al**
Unit cell parameters (Å), *a*, *b*, *c*	n.d.	12.170, 13.301, 10.005	n.d.	n.d.	11.815, 26.630, 10.042	n.d.
Volume (Å^3)	n.d.	1619.46	n.d.	n.d.	3159.55	n.d.
Optimized unit cell parameters (Å), *a*, *b*, *c*	12.0296, 13.2109, 9.9017	12.1698,* 13.3008, * 10.0048 *	11.7893, 13.4876, 10.1609	11.9479, 13.6593, 10.3157	11.8248, 26.7192, 10.0423	12.2217, 26.9351, 10.1760
Optimized volume (Å^3)	1573.60	1619.46	1615.68	1683.52	3172.86	3349.86
Z	4		4		8	
Energy per formula unit (eV)	–219.1885	–218.2701	–219.2479	–217.7659	–219.2780	–218.2109
FD [$(M + T)/1000$ Å^3]		19.76	19.81	19.01	22.69	21.49
v (atoms), framework, all	58, 60		116, 120		232, 240	
I_G (bits/atom), framework, all	3.892, 3.974		3.892, 3.974		4.858, 4.907	
$I_{G,\,total}$ (bits/unit cell), framework, all	225.763, 238.413		451.526, 476.827		1127.052, 1177.654	

n.d.—no data, because of the absence of structural information; original unit cell parameter.

As seen from the comparison between the original and optimized cells of $Cs\{Al_2[BP_6O_{20}]\}$ of the non-MDO 4*O* type, they are in a very good agreement, with the difference in volume of ca. 13 Å, i.e., ca. 0.4% (see Table 3). The optimized coordinates in all structures showed only minimal shifts from their original positions, mostly associated with a very small rotation of tetrahedra. It is important to note that, despite unconstrained optimization, all the structures, observed as well as hypothetical, retained their original cell symmetries.

As seen from Table 3, for the T = Al series, the structure with the lowest energy was the MDO1-type polytype. However, the non-MDO 4*O*-type structure was only ca. 0.06 eV higher in energy, which corresponds to ca. 6.2 kJ/mol. This difference is not large, yet is arguably outside the margin of error for the computational method used, which is commonly estimated as 1–2 kJ/mol. The important thing here is that both experimentally observed types of structures (albeit not both of them for T = Al), showed comparable energies. Moreover, our calculations indicate that, under the right conditions, it might be possible to obtain the non-MDO 4*O* polytype for aluminum. Regarding the MDO2-type structure, the optimization gave us a stable minimum structure with the energy of ca. 0.5 eV (ca. 49 kJ/mol) higher than MDO1. This means that, potentially, such a structure might exist, however, the energy difference to the lowest energy structure is significant, and thus it might be difficult to stabilize such a polytype.

For the T = B series, once again the lowest energy corresponds to the experimentally observed structure, this time it is the non-MDO 4*O* polytype (see Table 3). In this case, however, its energy is only ca. 0.03 eV (ca. 3 kJ/mol) lower than that of the hypothetical MDO2-type structure. The difference is on the border of the perceived accuracy of the computational method, thus the MDO2 polytype appears to be a good candidate for the experimental discovery. The MDO1-type structure in this case looks like the least favorable, energy-wise, with the difference between its energy and minimal structure being ca. 0.09 eV

(ca. 8.6 kJ/mol). This is clearly outside the margin of error; however, the difference is small enough to be compensated by various effects in real crystals. It must also be noted regarding all our calculations, that by their very nature they simulate ideal periodic crystals in their ground state at 0 K. In addition, in our computations we cannot account for potential kinetic hindrance of certain paths of compound formation.

4. Discussion

The heteropolyhedral *MT*-frameworks with similar stoichiometry (3) have been found in compounds with the general formula Rb{$^{[6]}M^{3+}{}_2[^{[4]}T^{3+}P_6O_{20}]$}, where *M* = Al, Ga; T = Al, Ga [26,56]. The unit cell parameters are similar to those for MDO1 and MDO2 polytypes of Cs{$Al_2[TP_6O_{20}]$} (*T* = Al, B): *a* = 9.876–10.002 Å; *b* = 12.885–13.082 Å; *c* = 11.919–12.071 Å; space group $C222_1$. Their crystal structures contain mixed tetrahedral $[TP_6O_{20}]$-chains, which are linked by the MO_6-octahedra (Figure 7). The tetrahedral chain is formed by the condensation of FBU, an open-branched heptamer with the descriptor 7□:[3□]2□|2□|□|□ similar to that for the tetrahedral $[TP_6O_{20}]$-layers in Cs{$Al_2[TP_6O_{20}]$} (*T* = Al, B). The negative charge of the framework is balanced by Rb^+ ions.

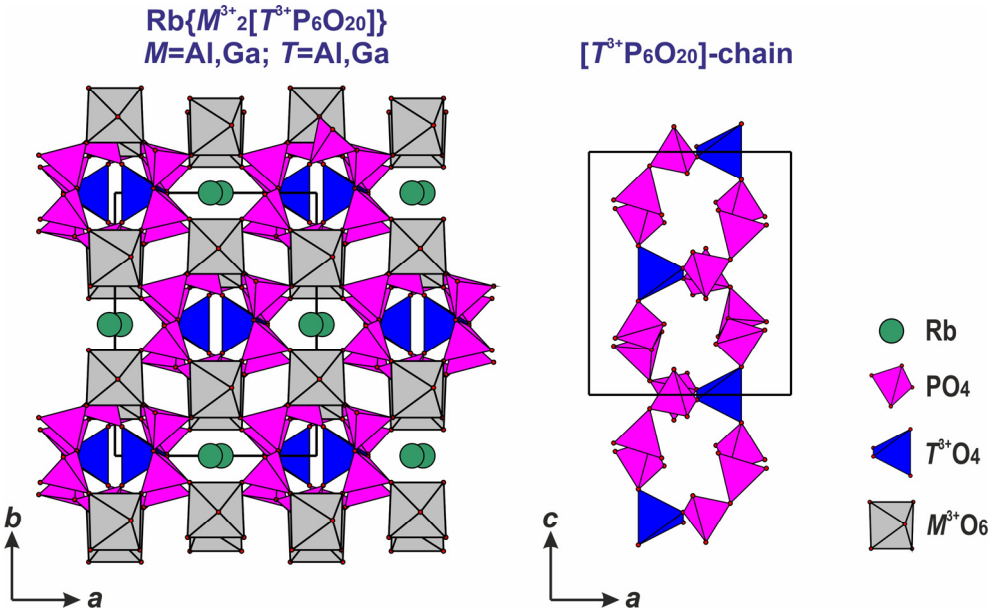

Figure 7. The general view of the crystal structure of compounds with the general formula Rb{$^{[6]}M^{3+}{}_2[^{[4]}T^{3+}P_6O_{20}]$} (where *M* = Al, Ga; *T* = Al, Ga [26,51]) and a tetrahedral chain going along [001].

Despite of the absence of the tetrahedral layers, the *MT*-framework can also be considered as the result of alternation along **b** of two types of nonpolar OD layers parallel to (010):

1. The first one corresponds to a layer with the symmetry $P2(2)2_1$ consisting of tetrahedral chains. The tetrahedral layer in Cs{$Al_2[TP_6O_{20}]$} and tetrahedral pseudolayer in Rb{$M_2[TP_6O_{20}]$ are formed by the same FBU and demonstrate the symmetrical relationship (Figure 8) indicating the possible OD-character as was previously shown for compounds with tetrameric [57] and pentameric [20] borophosphate FBUs, as well as for the silicate layers [58,59];
2. The second one consists of an octahedral layer with the symmetry $P2_1(2)2_1$ similar to that observed in Cs{$Al_2[TP_6O_{20}]$} (*T* = Al, B) (the layer group $P2_122_1$ is a subgroup of the layer group *Pcam*). To date, there are no other polytypes of this type of framework, however they may be found later.

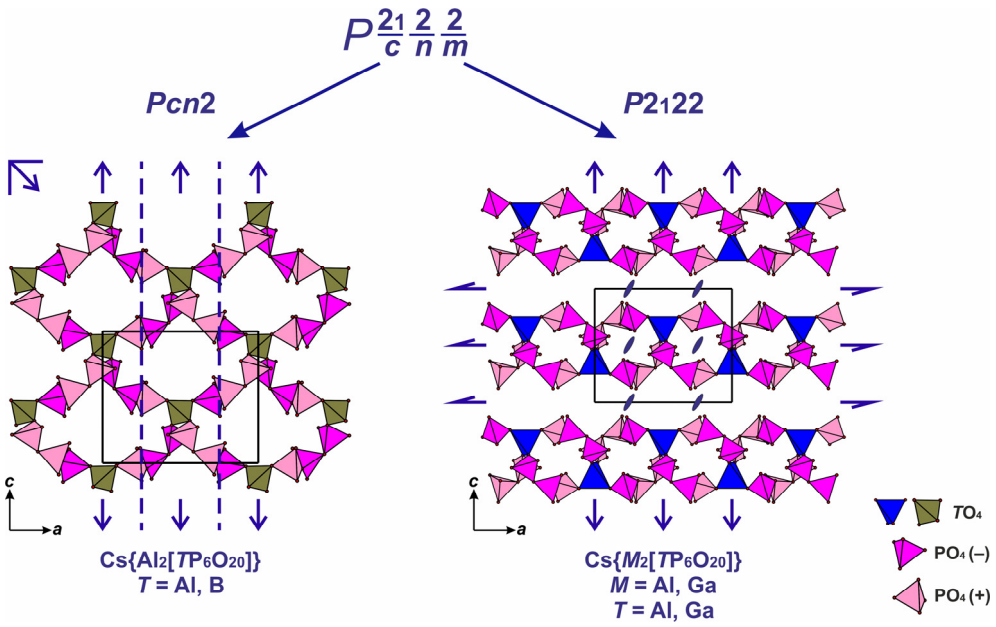

Figure 8. The symmetrical relationship between tetrahedral layers and tetrahedral pseudolayers in compounds with the general formulas $Cs\{Al_2[TP_6O_{20}]\}$ (T = Al, B) and $Rb\{M_2[TP_6O_{20}]\}$ (M = Al, Ga; T = Al, Ga), respectively. The orientation of the tetrahedral pseudolayer (right) have been changed using the [001/010/100] matrix in comparison with that in the crystal structures.

Topological features of the *MT*-framework are reflected in the sequence of its natural tiles: $[4.6^2]_2[4.7^2]_2[3.5.6^2]_2[3.4^2.5.7^2]_2[6^4.7^4]$. It should be noted that three tilings ($[4.6^2]$, $[4.7^2]$), and $[3.5.6^2]$) are topologically equivalent to those in the $Cs\{Al_2[TP_6O_{20}]\}$ (T = Al, B) compounds, which indicate the relation of the two types of the $\{^{[6]}M^{3+}{}_2[^{[4]}T^{3+}P_6O_{20}]\}$-frameworks.

5. Conclusions

The polytypism of compounds with the general formula $Cs\{Al_2[TP_6O_{20}]\}$ (T = Al, B) has been described using the OD theory approach. The crystal structure of the hypothetical MDO2 polytype has been proposed and optimized using DFT calculations. It was shown that the heteropolyhedral *MT*-frameworks of all the polytypes contain similar natural tilings. The compounds with the general formula $Rb\{^{[6]}M^{3+}{}_2[^{[4]}T^{3+}P_6O_{20}]\}$ (M = Al, Ga; T = Al, Ga) have the heteropolyedral *MT*-frameworks with the same stoichiometry. It was found that all the frameworks had common natural tilings, which indicates the relationship of both families of compounds. Our computational data agree well with those which are experimentally available and, we believe, provide a reasonable basis for an internally consistent picture which supports crystallographic considerations concerning the formation of the polytypes of compounds with the general formula $Cs\{Al_2[TP_6O_{20}]\}$ (T = Al, B). Thus, it is seems possible to synthesize the MDO2 polytype as well as the "missing" members, such as MDO1 polytype of $Cs\{Al_2[BP_6O_{20}]\}$ and non-MDO 4*O* polytype of $Cs\{Al_2[AlP_6O_{20}]\}$ using hydrothermal techniques.

Supplementary Materials: The following are available online at https://www.mdpi.com/article/10.3390/min11070708/s1, Table S1: Site coordinates (*xyz*) and site multiplicities (Mult.) for MDO2 polytype of $Cs\{Al_2[TP_6O_{20}]\}$. The optimized unit cell parameters and atomic coordinates for MDO1, MDO2, and non-MDO-4O polytypes of compounds with the general formula $Cs\{Al_2[TP_6O_{20}]\}$ (T = Al, B) are given (the atomic coordinates are given for the whole crystal structures for the space group *P*1).

Author Contributions: Conceptualization, S.M.A., A.N.K. and S.M.; formal analysis, S.M.A., A.A.A. and N.A.Y.; writing—review and editing, S.M.A. and S.M.; supervision, A.N.K., S.V.K. and S.M. All authors have read and agreed to the published version of the manuscript.

Funding: This research was funded by the Russian Science Foundation (Project No. 20-77-10065) (S.M.A., A.A.A.).

Acknowledgments: The authors are grateful to reviewers and the Special Issue editor Professor Giovanni Ferraris for their useful comments and suggestions.

Conflicts of Interest: The authors declare no conflict of interest.

References

1. Vinodkumar, P.; Panda, S.; Jaiganesh, G.; Padhi, R.K.; Madhusoodanan, U.; Panigrahi, B.S. SrBPO5: Ce^{3+}, Dy^{3+}—A cold white-light emitting phosphor. *Spectrochim. Acta Part. A Mol. Biomol. Spectrosc.* **2021**, *253*, 119560. [CrossRef]
2. He, X.; Hu, D.; Yang, G.; Adamietz, F.; Rodriguez, V.; Dussauze, M.; Fargues, A.; Fargin, E.; Cardinal, T. Microstructured SHG patterns on Sm_2O_3-doped borophosphate niobium glasses by laser-induced thermal poling. *Ceram. Int.* **2021**, *47*, 10123–10129. [CrossRef]
3. Joseph, P.A.J.; Maheshvaran, K.; Rayappan, I.A. Structural and optical studies on Dy^{3+} ions doped alkali lead borophosphate glasses for white light applications. *J. Non. Cryst. Solids* **2021**, *557*, 120652. [CrossRef]
4. Xiang, J.; Fang, Z.; Yang, D.; Zheng, Y.; Zhu, J. Optimizational orange emitting behavior of Li_2Na_1-BP_2O_8:xPr solid solutions under an short-wave ultraviolet irradiation. *Scr. Mater.* **2020**, *187*, 82–87. [CrossRef]
5. Zhao, D.; Cheng, W.-D.; Zhang, H.; Huang, S.-P.; Xie, Z.; Zhang, W.-L.; Yang, S.-L. $KMBP_2O_8$ (M = Sr, Ba): A New Kind of Noncentrosymmetry Borophosphate with the Three-Dimensional Diamond-like Framework. *Inorg. Chem.* **2009**, *48*, 6623–6629. [CrossRef]
6. Magistris, A.; Chiodelli, G.; Duclot, M. Silver borophosphate glasses: Ion transport, thermal stability and electrochemical behaviour. *Solid State Ion.* **1983**, *9–10*, 611–615. [CrossRef]
7. Mouyane, M.; Jumas, J.-C.; Olivier-Fourcade, J.; Cassaignon, S.; Jordy, C.; Lippens, P.-E. One-pot synthesis of tin-borophosphate-carbon composites as anode materials for Li-ion batteries. *J. Solid State Chem.* **2016**, *233*, 52–57. [CrossRef]
8. Yaghoobnejad Asl, H.; Stanley, P.; Ghosh, K.; Choudhury, A. Iron Borophosphate as a Potential Cathode for Lithium- and Sodium-Ion Batteries. *Chem. Mater.* **2015**, *27*, 7058–7069. [CrossRef]
9. Shenouda, A.Y.; Liu, H.K. Electrochemical behaviour of tin borophosphate negative electrodes for energy storage systems. *J. Power Sources* **2008**, *185*, 1386–1391. [CrossRef]
10. Shvanskaya, L.; Yakubovich, O.; Krikunova, P.; Ovchenkov, E.; Vasiliev, A. Chain caesium borophosphates with B:P ratio 1:2: Synthesis, structure relationships and low-temperature thermodynamic properties. *Acta Crystallogr. Sect. B Struct. Sci. Cryst. Eng. Mater.* **2019**, *75*, 1174–1185. [CrossRef] [PubMed]
11. Yakubovich, O.V.; Shvanskaya, L.V.; Kiriukhina, G.V.; Volkov, A.S.; Dimitrova, O.V.; Ovchenkov, E.A.; Tsirlin, A.A.; Shakin, A.A.; Volkova, O.S.; Vasiliev, A.N. Crystal structure and spin-trimer magnetism of $Rb_{2.3}(H_2O)_{0.8}Mn_3[B_4P_6O_{24}(O,OH)_2]$. *Dalt. Trans.* **2017**, *46*, 2957–2965. [CrossRef]
12. Shvanskaya, L.; Yakubovich, O.; Melchakova, L.; Ivanova, A.; Vasiliev, A. Crystal chemistry and physical properties of the $A_2M_3(H_2O)_2[B_4P_6O_{24}(OH)_2]$ (A = Cs, Rb; M = Ni, Cu, (Ni, Fe)) borophosphate family. *Dalt. Trans.* **2019**, *48*, 8835–8842. [CrossRef] [PubMed]
13. Scheide, M.R.; Peterle, M.M.; Saba, S.; Neto, J.S.S.; Lenz, G.F.; Cezar, R.D.; Felix, J.F.; Botteselle, G.V.; Schneider, R.; Rafique, J.; et al. Borophosphate glass as an active media for CuO nanoparticle growth: An efficient catalyst for selenylation of oxadiazoles and application in redox reactions. *Sci. Rep.* **2020**, *10*, 15233. [CrossRef] [PubMed]
14. Matzkeit, Y.H.; Tornquist, B.L.; Manarin, F.; Botteselle, G.V.; Rafique, J.; Saba, S.; Braga, A.L.; Felix, J.F.; Schneider, R. Borophosphate glasses: Synthesis, characterization and application as catalyst for bis(indolyl)methanes synthesis under greener conditions. *J. Non. Cryst. Solids* **2018**, *498*, 153–159. [CrossRef]
15. Wang, B.; Lu, W.-X.; Huang, Z.-Q.; Chen, W.-J.; Xie, J.-L.; Pan, D.-S.; Zhou, L.-L.; Song, J.-L. Amorphous N-Doped Cobalt Borophosphate Nanoparticles as Robust and Durable Electrocatalyst for Water Oxidation. *ACS Sustain. Chem. Eng.* **2019**, *7*, 13981–13988. [CrossRef]
16. Belokoneva, E.L.; Dimitrova, O.V. $Fe_{2.5}[BP_2O_7(OH)_2][PO_3(OH)][PO_3(O_{0.5}OH_{0.5})] \cdot H_2O$, a new phosphate-borophosphate with a microporous structure. *Crystallogr. Rep.* **2015**, *60*, 361–366. [CrossRef]
17. Yang, M.; Yan, P.; Xu, F.; Ma, J.; Welz-Biermann, U. Role of boron-containing ionic liquid in the synthesis of manganese borophosphate with extra-large 16-ring pore openings. *Microporous Mesoporous Mater.* **2012**, *147*, 73–78. [CrossRef]
18. Kang, Q.-Y.; Song, Q.; Li, S.-Y.; Liu, Z.-H. Thermodynamic properties of microporous materials for two borophosphates, $K[ZnBP_2O_8]$ and $NH4[ZnBP_2O_8]$. *J. Chem. Thermodyn.* **2014**, *69*, 43–47. [CrossRef]
19. Yang, T.; Li, G.; Ju, J.; Liao, F.; Xiong, M.; Lin, J. A series of borate-rich metalloborophosphates $Na_2[M^{II}B_3P_2O_{11}(OH)]$ $0.67H_2O$ (M^{II}=Mg, Mn, Fe, Co, Ni, Cu, Zn): Synthesis, structure and magnetic susceptibility. *J. Solid State Chem.* **2006**, *179*, 2534–2540. [CrossRef]
20. Aksenov, S.M.; Yamnova, N.A.; Borovikova, E.Y.; Stefanovich, S.Y.; Volkov, A.S.; Deyneko, D.V.; Dimitrova, O.V.; Hixon, A.E.; Krivovichev, S.V. Topological features of borophosphates with mixed frameworks. Synthesis, crystal structure of $Li_3\{Al_2[BP_4O_{16}]\}\cdot 2H_2O$, and comparative crystal chemistry. *J. Struct. Chem.* **2020**, *61*. [CrossRef]

21. Ewald, B.; Huang, Y.-X.; Kniep, R. Structural Chemistry of Borophosphates, Metalloborophosphates, and Related Compounds. *Z. Anorg. Allg. Chem.* **2007**, *633*, 1517–1540. [CrossRef]
22. Gurbanova, O.A.; Belokoneva, E.L. Comparative crystal chemical analysis of borophosphates and borosilicates. *Crystallogr. Rep.* **2007**, *52*, 624–633. [CrossRef]
23. Li, M.; Verena-Mudring, A. New Developments in the Synthesis, Structure, and Applications of Borophosphates and Metalloborophosphates. *Cryst. Growth Des.* **2016**, *16*, 2441–2458. [CrossRef]
24. Yakubovich, O.; Steele, I.; Massa, W. Genetic aspects of borophosphate crystal chemistry. *Z. Krist. Cryst. Mater.* **2013**, *228*. [CrossRef]
25. Shvanskaya, L.V.; Yakubovich, O.V.; Belik, V.I. New type of borophosphate anionic radical in the crystal structure of CsAl2BP6O20. *Crystallogr. Rep.* **2016**, *61*, 786–795. [CrossRef]
26. Lesage, J.; Guesdon, A.; Raveau, B. Two aluminotriphosphates with closely related intersecting tunnel structures involving tetrahedral "AlP" chains and layers: $AAl_3(P_3O_{10})_2$, A=Rb, Cs. *J. Solid State Chem.* **2005**, *178*, 1212–1220. [CrossRef]
27. Ferraris, G.; Makovicky, E.; Merlino, S. *Crystallography of Modular Materials*; Oxford University Press: Oxford, UK, 2008; ISBN 9780191712111.
28. Dornberger-Schiff, K. Grundzüge einer Theorie der OD-Strukturen aus Schichten. *Abh. Dtsch. Akad. Wiss. Berlin. Kl. Chem. Geol. Biol.* **1964**, *3*, 1–107.
29. Dornberger-Schiff, K. *Lehrgang Über OD-Strukturen*; Akademie-Verlag: Berlin, Germany, 1966.
30. Dornberger-Schiff, K.; Grell-Niemann, H. On the theory of order–disorder (OD) structures. *Acta Crystallogr.* **1961**, *14*, 167–177. [CrossRef]
31. Dornberger-Schiff, K.; Grell, H. Geometrical properties of MDO polytypes and procedures for their derivation. II. OD families containing OD layers of M > 1 kinds and their MDO polytypes. *Acta Crystallogr. Sect. A* **1982**, *38*, 491–498. [CrossRef]
32. Grell, H. How to choose OD layers. *Acta Crystallogr. Sect. A Found. Crystallogr.* **1984**, *40*, 95–99. [CrossRef]
33. Blatov, V.A.; O'Keeffe, M.; Proserpio, D.M. Vertex-, face-, point-, Schläfli-, and Delaney-symbols in nets, polyhedra and tilings: Recommended terminology. *Cryst. Eng. Comm.* **2010**, *12*, 44–48. [CrossRef]
34. Krivovichev, S.V. Structural and topological complexity of zeolites: An information-theoretic analysis. *Microporous Mesoporous Mater.* **2013**, *171*, 223–229. [CrossRef]
35. Krivovichev, S.V. Which inorganic structures are the most complex? *Angew. Chem. Int. Ed.* **2014**, *53*, 654–661. [CrossRef]
36. Blatov, V.A.; Ilyushin, G.D.; Blatova, O.A.; Anurova, N.A.; Ivanov-Schits, A.K.; Dem'yanets, L.N. Analysis of migration paths in fast-ion conductors with Voronoi–Dirichlet partition. *Acta Crystallogr. Sect. B Struct. Sci.* **2006**, *62*, 1010–1018. [CrossRef]
37. Anurova, N.A.; Blatov, V.A.; Ilyushin, G.D.; Blatova, O.A.; Ivanov-Schits, A.K.; Dem'yanets, L.N. Migration maps of Li^+ cations in oxygen-containing compounds. *Solid State Ion.* **2008**, *179*, 2248–2254. [CrossRef]
38. Eremin, R.A.; Kabanova, N.A.; Morkhova, Y.A.; Golov, A.A.; Blatov, V.A. High-throughput search for potential potassium ion conductors: A combination of geometrical-topological and density functional theory approaches. *Solid State Ion.* **2018**, *326*, 188–199. [CrossRef]
39. Blatov, V.A.; Shevchenko, A.P.; Proserpio, D.M. Applied Topological Analysis of Crystal Structures with the Program Package ToposPro. *Cryst. Growth Des.* **2014**, *14*, 3576–3586. [CrossRef]
40. Perdew, J.P.; Burke, K.; Ernzerhof, M. Generalized Gradient Approximation Made Simple. *Phys. Rev. Lett.* **1996**, *77*, 3865–3868. [CrossRef] [PubMed]
41. Kresse, G.; Joubert, D. From ultrasoft pseudopotentials to the projector augmented-wave method. *Phys. Rev. B* **1999**, *59*, 1758–1775. [CrossRef]
42. Kresse, G.; Furthmüller, J. Vienna Ab-initio Simulation Package (VASP), V.5.4.4. Available online: www.vasp.at (accessed on 25 June 2021).
43. Monkhorst, H.J.; Pack, J.D. Special points for Brillouin-zone integrations. *Phys. Rev. B* **1976**, *13*, 5188–5192. [CrossRef]
44. Dornberger-Schiff, K. On the nomenclature of the 80 plane groups in three dimensions. *Acta Crystallogr.* **1959**, *12*, 173. [CrossRef]
45. Burns, P.C.; Grice, J.D.; Hawthorne, F.C. Borate minerals. I. Polyhedral clusters and foundamental building block. *Can. Mineral.* **1995**, *33*, 1131–1151.
46. Grell, H.; Dornberger-Schiff, K. Symbols for OD groupoid families referring to OD structures (polytypes) consisting of more than one kind of layer. *Acta Crystallogr. Sect. A* **1982**, *38*, 49–54. [CrossRef]
47. Ďurovič, S. Desymmetrization of OD Structures. *Krist. Tech.* **1979**, *14*, 1047–1053. [CrossRef]
48. Merlino, S. *EMU Notes in Mineralogy. Vol. 1. Modular Aspects of Minerals*; Merlino, S., Ed.; Eötvös University Press: Budapest, Hungary, 1997.
49. Rocha, J.; Lin, Z. Microporous Mixed Octahedral-Pentahedral-Tetrahedral Framework Silicates. *Rev. Mineral. Geochem.* **2005**, *57*, 173–201. [CrossRef]
50. Chukanov, N.V.; Pekov, I.V.; Rastsvetaeva, R.K. Crystal chemistry, properties and synthesis of microporous silicates containing transition elements. *Russ. Chem. Rev.* **2004**, *73*, 205–223. [CrossRef]
51. Chukanov, N.V.; Pekov, I.V. Heterosilicates with Tetrahedral-Octahedral Frameworks: Mineralogical and Crystal-Chemical Aspects. *Rev. Mineral. Geochem.* **2005**, *57*, 105–143. [CrossRef]
52. Baerlocher, C.; McCusker, L.B. Database of Zeolite Structures. Available online: http://www.iza-structure.org/databases/ (accessed on 25 June 2021).

53. Voronkov, A.A.; Ilyukhin, V.V.; Belov, N.V. Crystal chemistry of mixed frameworks—Principles of their formation. *Kristallografiya* **1975**, *20*, 556–566.
54. Sandomirskiy, P.A.; Belov, N.V. *Crystal Chemistry of Mixed Anionic Radicals*; Nauka: Moscow, Russia, 1984.
55. Ilyushin, G.D.; Blatov, V.A. Crystal chemistry of zirconosilicates and their analogs: Topological classification of MT frameworks and suprapolyhedral invariants. *Acta Crystallogr. Sect. B Struct. Sci.* **2002**, *58*, 198–218. [CrossRef]
56. Lesage, J.; Guesdon, A.; Raveau, B. $RbGa_3$ $(P_3O_{10})_2$: A new gallium phosphate isotypic with $RbAl_3(P_3O_{10})_2$. *Acta Crystallogr. Sect. C Cryst. Struct. Commun.* **2005**, *61*, i44–i46. [CrossRef]
57. Ruchkina, E.A.; Belokoneva, E.L. Structural features of lead iron borophosphates of alkali metals as analyzed in terms of topologically similar structural blocks. *Russ. J. Inorg. Chem.* **2003**, *48*, 1969–1978.
58. Topnikova, A.; Belokoneva, E.; Dimitrova, O.; Volkov, A.; Deyneko, D. $Rb_{1.66}Cs_{1.34}Tb[Si_{5.43}Ge_{0.57}O_{15}]$·H2O, a New Member of the OD-Family of Natural and Synthetic Layered Silicates: Topology-Symmetry Analysis and Structure Prediction. *Minerals* **2021**, *11*, 395. [CrossRef]
59. Belokoneva, E.L.; Reutova, O.V.; Dimitrova, O.V.; Volkov, A.S. Germanosilicate $Cs_2In_2[(Si_{2.1}Ge_{0.9})_2O_{15}](OH)_2$ H_2O with a New Corrugated Tetrahedral Layer: Topological Symmetry-Based Prediction of Anionic Radicals. *Crystallogr. Rep.* **2020**, *65*, 566–572. [CrossRef]